High strength $Mg_{94}Zn_{2.4}Y_{3.6}$ alloy with long period stacking ordered structure prepared by near-rapid solidification technology

J. Zhu[a], J.B. Chen[a], T. Liu[a], J.X. Liu[b], W.Y. Wang[c], Z.K. Liu[c], X.D. Hui[a],*

[a] State Key Laboratory for Advanced Metals and Materials, University of Science and Technology Beijing, Beijing 100083, China
[b] Department of ENT, Peking University Third Hospital, Beijing 10191, China
[c] Department of Materials Science and Engineering, The Pennsylvania State University, University Park, PA 16802, USA

ARTICLE INFO

ABSTRACT

To obtain high strength for near-rapid solidification (NRS) magnesium alloys, the microstructures and mechanical properties of the $Mg_{94}Zn_{2.4}Y_{3.6}$ (at%) alloys, which were prepared by ordinary and injection copper mold casting (ICMC), respectively, were investigated comprehensively. It has been shown that the microstructure of ICMC $Mg_{94}Zn_{2.4}Y_{3.6}$ alloy possesses the far-away-from equilibrium feature of NRS materials, which is composed of refined α-Mg grains with supersaturated Y and Zn, fine network-like long-period stacking-order (LPSO) phases and a few of $Mg_{24}Y_5$ particles. The interface between LPSO phase and α-Mg matrix is semi-coherent with the orientation relationship of $[0002]_α//[11\overline{2}0]_{LPSO}$, $(10\overline{1}0)_α//(0002)_{LPSO}$. The ICMC alloy exhibits enhanced mechanical properties with the ultimate tensile strength and elongation up to 355 MPa and 7% at room temperature, respectively, and with the ultimate tensile strength of 302 MPa at 150 °C. It can be concluded that the strengthening mechanisms of this ICMC alloy are attributed to the grain refinement, the solid solution effect, the secondary phase strengthening and the crystalline boundaries strengthening.

1. Introduction

Magnesium alloys have been broadly applied in many engineering fields due to their low density, high specific strength, recyclability and easy machinability [1–4]. However, the low strength and poor plasticity of magnesium alloys seriously limits their application, especially at the elevated temperature. Thus pursuing for high strength and plasticity has been remained as an important issue for magnesium alloys in recent years [5–7].

It is well known that grain refinement is one of the most effective ways to improve the strength of metallic materials through Hall-Petch relationship [8]. The solidification under a high cooling rate could result in fine microstructure as well as other merits such as the decreased segregation, the supersaturated solid solution of solute elements and the formation of metastable or amorphous phases [9]. Therefore, rapid solidified magnesium alloys have attracted great attention recently because of their high mechanical properties at room and elevated temperature [10–14]. In 2001, $Mg_{97}Zn_1Y_2$ alloy with the tensile yield strength exceeding 600 MPa, which was prepared by rapidly solidified powder metallurgy (RS/PM) technology, was reported by Kawamura et al. The excellent properties were attributed to the combination of fine grain size and novel long-period stacking-

order (LPSO) phases [10,11]. The LPSO structure has a long range stacking of basal hexagonal planes with periodic enrichment of Y and Zn atoms in particular atomic planes [15]. Until now, four types of LPSO structures have been found in Mg–Zn–Y alloys [16,17], including 10H, 18R, 14H and 24R. The stacking order of 18R structure in Mg–Zn–Y alloys was supposed to be the same as that of an equilibrium X–$Mg_{12}ZnY$ phase [18]. It has been proved that X–$Mg_{12}ZnY$ phase plays a critical role for the superior mechanical properties of Mg–Zn–Y alloys [19,20].

Although rapid solidification process could render magnesium alloys high strength, subsequent powder metallurgy (PM) [11,13] or hot extrusion [21–23] will be needed to form the bulk alloys. Therefore, RS/PM magnesium alloys are usually more expensive and their preparation periods are longer than that of die cast Mg alloys. That's why most of magnesium alloy parts are currently produced by die casting but not RS/PM technology. The die cast (DC) is a circular process, which is usually conducted at the temperature 200–280 °C and the solidification rate is lower than 1 K/s [1]. Therefore, the DC Mg alloys usually contain coarse dendrites, and their mechanical properties are relatively low. To overcome these drawbacks, rheocasting processing has been extensively investigated for magnesium alloys. However, the strengths of magnesium alloys prepared by traditional

* Corresponding author.
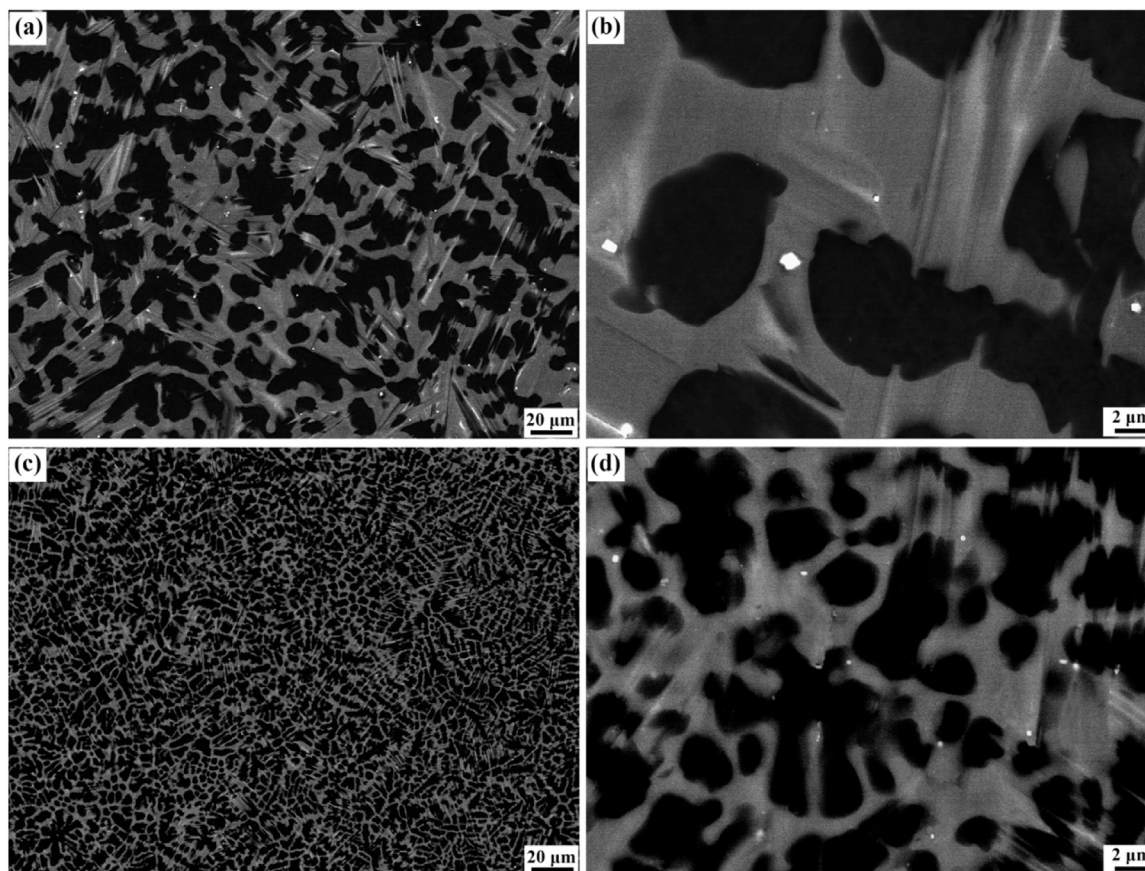   E-mail address: xdhui@ustb.edu.cn (X.D. Hui).

Fig. 1. SEM back scattered electron images of the Mg$_{94}$Zn$_{2.4}$Y$_{3.6}$ alloy samples: (a) and (b) CMC alloy; (c) and (d) ICMC alloy.

die casting still need urgently to be improved.

For a long time, the near-rapid solidification (NRS) of Mg alloys under the cooling rate from 1 K/s to 10^3 K/s has not been sufficiently investigated. Under the NRS condition, far-away-from equilibrium microstructure for many metallic materials may be formed [24]. Nowadays, this technology has become an important way to obtain miraculous microstructure and properties for materials. In some extreme case, some alloys can even be solidified into quasicrystalline or amorphous structure. In present work, a high strength Mg$_{94}$Zn$_{2.4}$Y$_{3.6}$ (at%) alloy with LPSO structure is prepared by injection copper mold casting (ICMC) technology. For comparison, thick rod-like samples were also casted by copper mold casting (CMC). The mechanical properties of these two kinds of alloys are tested at room and elevated temperature. The microstructures and strengthening mechanisms are investigated by TEM and HRTEM studies. The ICMC technology used in this work is similar to the die casting in principle, while its cooling rate falls into the scope of NRS technology. Therefore, the knowledge of microstructures, mechanical properties and strengthening mechanisms of ICMC alloys is significant for the composition design and the cast processing of high strength magnesium alloys.

2. Experimental procedures

The master alloy ingots of Mg$_{94}$Zn$_{2.4}$Y$_{3.6}$ (at%) was prepared by medium frequency induction melting using pure metals of Mg (99.90 wt%), Zn (99.99 wt%) and the medium alloys of Mg–Y using graphite crucible in an argon atmosphere. Then one part of the master alloy ingot was remelted and poured into a water-cooled copper mold to cast cylindrical samples with the diameter of 25 mm. In this work, the master alloy ingot was also remelted in a quartz tube using high frequency induction melting in a purified inert atmosphere, and then injected into a water-cooled copper mold with the internal rod-shaped

cavity of 3 mm in diameter and 70 mm in length. For convenience, the samples prepared by pouring and injection copper mold casting are named as CMC and ICMC alloy, respectively, in the following contest.

The cooling rates during these two solidification processes can be evaluated by finite element calculation. According to simulation results of Inoue et al. [25], the cooling rates of Mg-Cu-Y rods are 180 K/s and < 1 K/s, respectively, when the diameters of the cast rods are 3 mm and 25 mm. Therefore, in this work, the solidification processes of CMC and ICMC samples with the diameter of 25 mm and 3 mm can be classified into ordinary cast and near-rapid solidification (NRS), respectively.

The as-cast rods were analyzed by an X-ray diffraction (XRD, PHILIPS APD-10) with a monochromatic Cu K$_\alpha$ radiation to identify the phase compositions. The microstructures and morphologies of these alloy rods were observed by a scanning electronic microscopy (SEM, ZEISS SUPRA55) operated in the back-scattering electron (BSE) mode. The statistical analyses for the distribution of the phase grain sizes were performed based on the BSE images by using the professional grain size measurement software named Nano Measurer. Four different BSE images were selected for CMC and ICMC alloy, respectively, to ensure the validity of the experimental results. And then 100 grain samples in each BSE image were randomly selected to measure the α-Mg grain sizes or thicknessess of the network-Mg$_{12}$ZnY compound. The refined microstructure of the ICMC alloy was further studied by transmission electron microscopy (TEM) and selected area electron diffraction (SAED) through a Tecnai G2 F30 S-TWIN instrument operated at 200 kV. The specimens for TEM study were prepared by electrolytic polishing in an electrolyte containing 3 (vol%) perchloric acid and 97 (vol%) ethanol at 30 V, using an automatic twin-jet electro polisher. The temperature of the electrolyte during polishing was maintained at −35 ℃.

The room temperature tensile tests were carried out at a strain rate of 5×10^{-4} s^{-1} by a DDL-50 testing machine. The elevated temperature
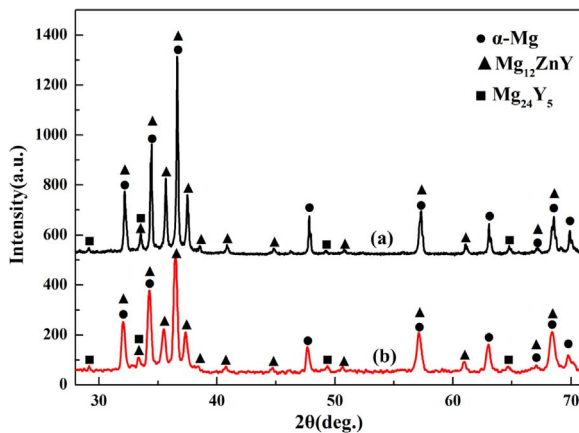
Fig. 2. X-ray diffraction patterns of the $Mg_{94}Zn_{2.4}Y_{3.6}$ samples prepared by different technology: (a) CMC and (b) ICMC alloy.

tensile tests were carried out at a strain rate of 5×10^{-4} s^{-1} at 150 ºC using a DDL-50 testing machine. Before elevated temperature tensile tests, the samples were held for 10 min at 150 ºC in the furnace. The diameters and gauge lengths of tensile specimens are 2 mm and 10 mm, respectively. The fracture morphologies of the as-cast samples were characterized by scanning electron microscopy (SEM, ZEISS SUPRA55).

3. Results

3.1. Phase compositions and microstructures

The SEM images and XRD patterns of $Mg_{94}Zn_{2.4}Y_{3.6}$ alloy under different solidification conditions are shown Figs. 1 and 2, respectively. From Fig. 1(a) and (b), it is seen that the microstructure of the CMC alloy is composed of three phases, which are distinguished by black dendrites, gray interdendritic networks and tiny white particles. From the typical XRD pattern in Fig. 2(a), it is identified that the CMC alloy is mainly composed of α-Mg, $Mg_{12}ZnY$ and $Mg_{24}Y_5$ phase. To further identify the types of these phases, we performed an Energy Dispersive Spectrometer (EDS) analysis as shown in Fig. 3. The chemical compositions listed in Table 1 confirm that the black, gray and white phases are α-Mg, $Mg_{12}ZnY$ and $Mg_{24}Y_5$ phases, respectively. According to the liquidus surface of Mg–Zn–Y ternary system [26,27], there exists a binary reaction: L→α-Mg+$Mg_{12}ZnY$ at the composition of 94 at% Mg, 2.4 at% Zn and 3.6 at% Y. The formation of tiny and scanty $Mg_{24}Y_5$ particle is mainly due to the segregation of Y element. For the ICMC alloy, the microstructure (Figs. 1(c), (d) and 2(b)) is also composed of α-Mg dendrites, interdendritic network-$Mg_{12}ZnY$ compounds and a few of tiny $Mg_{24}Y_5$ particles. As shown in Fig. 1(b) and (d), $Mg_{24}Y_5$ particles distribute in the matrix or at the grain boundaries of $Mg_{12}ZnY$ phases. It is notable that the $Mg_{24}Y_5$ particles in ICMC alloy are so fine that it couldn't be differentiated clearly in Fig. 1(c).

The non-equilibrium solidification is beneficial to the decrease of composition segregation and the enhancement in the supersaturation of solid solution phases. These features can be revealed from the distribution of elements in different phases. According to the Mg–Y binary phase diagram, the solubility of Y element in α-Mg is very low at room temperature. As shown in Table 1, the α-Mg solid solution in ICMC $Mg_{94}Zn_{2.4}Y_{3.6}$ alloy contains 0.8 at% Zn and 2.1 at% Y, which surpasses the solubility of Zn and Y in α-Mg. Moreover, compared with α-Mg phase in CMC alloy, the α-Mg phase in ICMC alloy contains more Zn and Y, indicating that near rapid cooling is beneficial to the supersaturation. It is also noticed that the white phase contains all the three elements, and the summation of Y and Zn content is nearly equal to the stoichiometric Y content (17.2 at%) of $Mg_{24}Y_5$. This means that some positions of Y atoms are replaced by Zn atoms in $Mg_{24}Y_5$

particle. In Table 1, it is shown that the Zn content in the gray phase of the CMC and ICMC alloys are lower than the stoichiometric concentration of Y (7.1 at%) in $Mg_{12}ZnY$ compound, and the Y/Zn atomic ratio is about 1.44 instead of the stoichiometric ratio of 1.0 in $Mg_{12}ZnY$ compound.

From Fig. 1, it is observed that the microstructure of ICMC alloy is much more refined than that of CMC alloy. The statistical distribution of the phase grain sizes in the two kinds of cast alloys are shown in Fig. 4. It is seen that both the grain size of α-Mg and thickness of $Mg_{12}ZnY$ decrease exponentially with the increase of cooling rate. As shown in Fig. 4(b), the fractions of α-Mg with the grain size lower than 9 μm and 3 μm reach up to 92.3% and 41.5%, respectively. In CMC alloy as shown by Fig. 4(a), however, α-Mg grain with the size lower than 3 μm was hardly formed and the α-Mg grains with the size of lower than 9 μm only take account of about 14%. As shown in Fig. 4(d), the thickness of all $Mg_{12}ZnY$ grains in the ICMC alloy is less than 5 μm, and the fraction of $Mg_{12}ZnY$ with the thickness lower than 2 μm in this sample is about 85%. It is also found that most of $Mg_{12}ZnY$ grains in ICMC alloy is in the range of 0–1.5 μm, whereas all of those in CMC alloy is larger than 1.5 μm as shown by Fig. 4(c).

3.2. TEM study of ICMC alloy

TEM investigations of the ICMC $Mg_{94}Zn_{2.4}Y_{3.6}$ alloy were performed in this alloy. It is seen from Fig. 5(a) that the microstructure of ICMC alloy is mainly consisted of matrix and thin reticular phase. In addition, a cuboid particle with a diameter of about 300 nm is precipitated in the reticular phase. The select area electron diffraction (SAED) pattern of matrix (marked as area A), as shown in Fig. 5(b), confirms that the matrix is hexagonal structure of α-Mg (a=0.321 nm, c=0.521 nm). In Fig. 5(c), it is seen that there are weaker spots at the positions n/6 (where *n* is an integer) of the $(0002)_{Mg}$ diffraction pattern, indicating that the phase in area B is an 18 R LPSO phase (a=0.321 nm, c=4.86 nm) [28,29]. The cuboid particle (area C) is identified as the body-centered cubic (bcc) $Mg_{24}Y_5$ phase (a=1.022 nm), as shown by Fig. 5(d) and (e).

To further explore the refined structures of $Mg_{12}ZnY$ and $Mg_{24}Y_5$ phase, high resolution transmission electron microscopy (HRTEM) analyses were carried out. As shown in Fig. 6(a), it is recognized that the structure of $Mg_{12}ZnY$ phase consists of two types of fringe regions with different intervals along the *c*-axis direction. The fringe spacings of these regions are carefully measured to be 1.6 nm and 2.3 nm, respectively. It was previously reported that the finger spacing of 18 R structure is 1.6 nm [30]. Moreover, the fringe with the wider spacing is the image of stacking fault (SF). Therefore, it is found in this work that the $Mg_{12}ZnY$ phase is not a monolithic LPSO structure, but a composite of 18R LPSO and SF. A local region containing both 18R LPSO and SF, as indicated by the rectangular frame in Fig. 6(a), is magnified and presented in Fig. 6(b). It is seen that the stacking sequence of the 18R LPSO is ABABABCACACABCBCBC with a period of 4.86 nm along the *c*-axis direction in Fig. 6(b) [16]. And each LPSO is composed of three successive building blocks with the same shear direction as indicated by the purple lines (Fig. 6(b)). Because the 18R LPSO is separated by a band of SF, it is seen that the building blocks of 18R LPSO on the two sides of the SF have opposite stacking sequences.

As shown in Fig. 6(c), it is seen that $Mg_{12}ZnY$ compound was precipitated from the α-Mg matrix. The orientation relation between α-Mg matrix and LPSO compound can be expressed as $[0002]_{α}//[11\bar{2}0]_{LPSO}$, $(10\bar{1}0)_{α}//(0002)_{LPSO}$. The lattice mismatch between $(10\bar{1}0)_{α}$ and $(0002)_{LPSO}$ is 5.9%, which is higher than 5% but lower than 10%. Therefore, the interface between α-Mg matrix and LPSO compound is semi-coherent. As shown in Fig. 6(d), the interplanar crystal spacing of (110) of $Mg_{24}Y_5$ phase (marked as C in Fig. 5(a)) is 0.716 nm. According to this interplanar crystal spacing and the SAED patterns (Fig. 5(d) and (e)), the lattice constant of $Mg_{24}Y_5$ phase can be calculated to be 1.022 nm which is lower than the previous reported
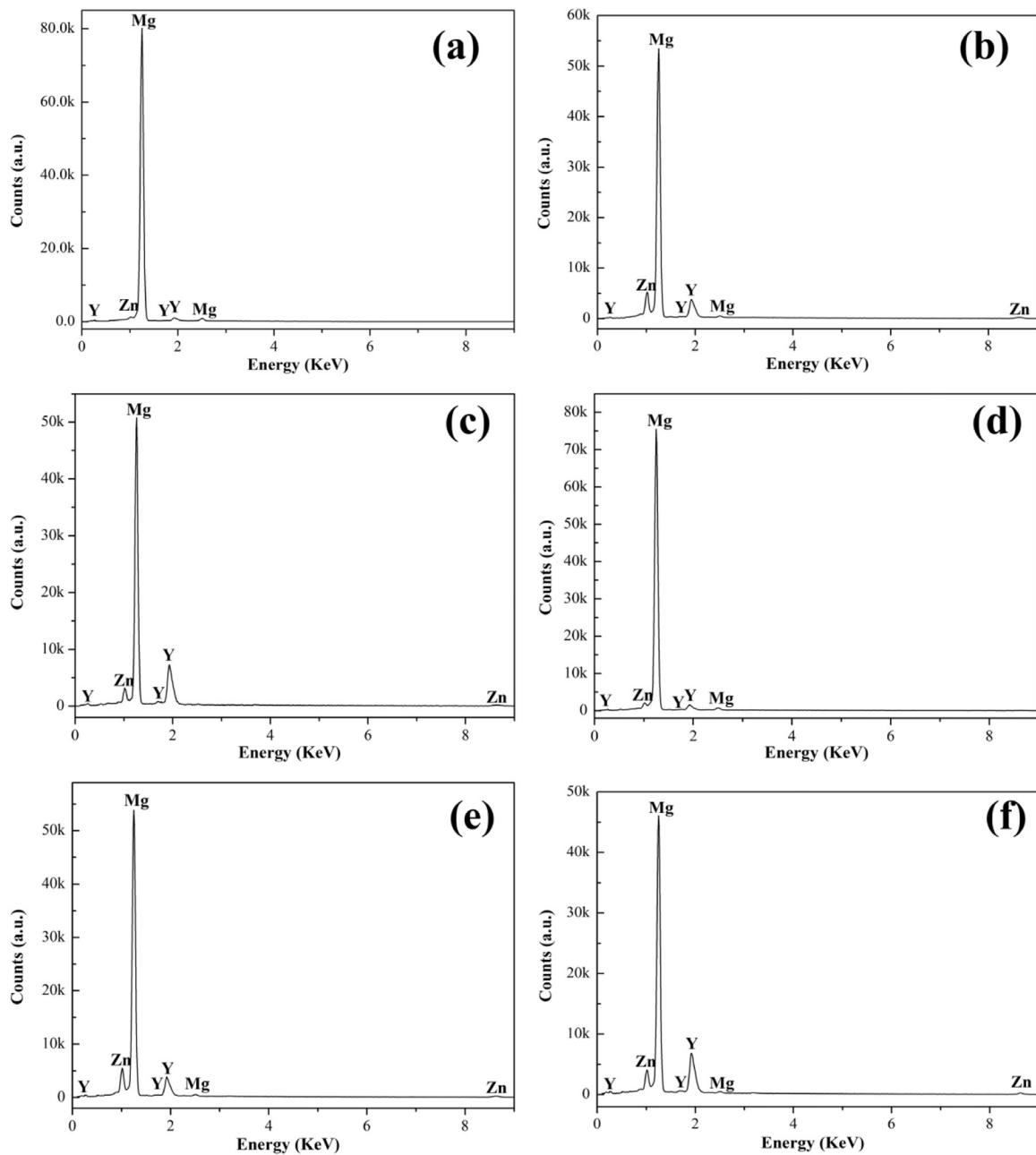
Fig. 3. EDS patterns of (a) black matrix, (b) gray network phase and (c) white particle in the CMC alloy; EDS patterns of (d) black matrix, (e) gray network phase and (f) white particle in the ICMC alloy.

Table 1
EDS results for the phases in the $Mg_{94}Zn_{2.4}Y_{3.6}$ alloys prepared by different technology.

Alloy	Phase	Mg (at%)	Zn (at%)	Y (at%)
Φ25×100 mm rod	Black	97.9	0.6	1.5
	Gray	88.3	4.8	6.9
	White	83.1	3.3	13.6
Φ3×70 mm rod	Black	97.1	0.8	2.1
	Gray	87.6	5.1	7.3
	White	82.6	3.6	13.8

1.12 nm [31]. This reduction of lattice constant is because that at some positions in $Mg_{24}Y_5$ phase, lager Y atoms were replaced by smaller Zn atoms (as listed in Table 1). The orientation relation between LPSO compound and $Mg_{24}Y_5$ phase (indicated by Z) can be concluded to $[0002]_{LPSO}//[001]_Z$, $(10\bar{1}0)_{LPSO}//(110)_Z$. The lattice mismatch between

$(10\bar{1}0)_{LPSO}$ and $(110)_Z$ is about 87%, meaning that the interface between LPSO phase and $Mg_{24}Y_5$ particle is incoherent.

3.3. Mechanical properties of the cast Mg–Zn–Y alloys

The engineering tensile stress-strain curves of the CMC and ICMC samples tested at room temperature and 150 °C are shown in Fig. 7. It is found that significant improvement in mechanical properties of the ICMC $Mg_{94}Zn_{2.4}Y_{3.6}$ alloy has been achieved due to the increase of cooling rate in comparison with the CMC sample. As shown in Fig. 7(b), the yield and ultimate tensile strength of ICMC sample reaches up to 236 MPa and 355 MPa, respectively, which are about 1.5 times as those of CMC sample, and are better than those of most of conventional magnesium alloys. It is found that the ICMC alloy possesses good plasticity, with the plastic elongation up to 7%. It is noticeable that the elevated temperature mechanical properties of
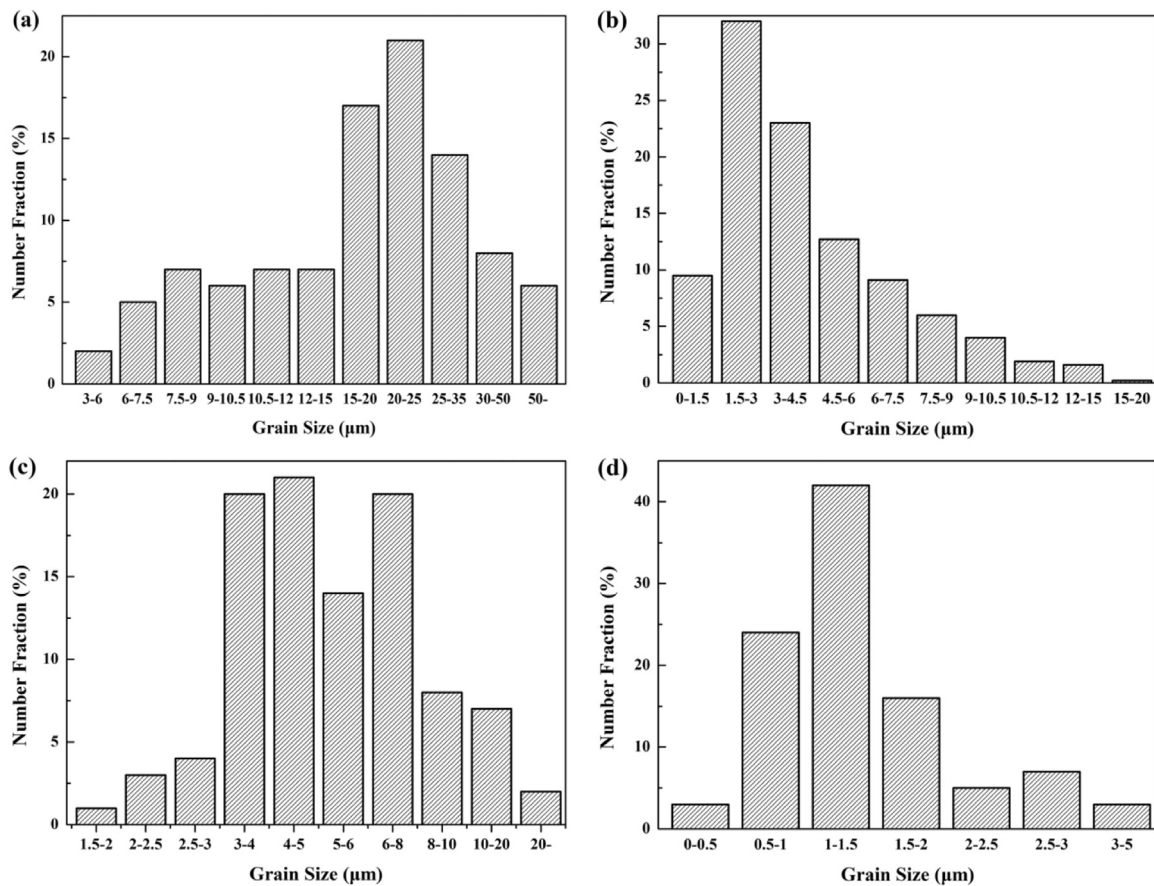
Fig. 4. The statistical distributions of the phase grain sizes in the two kinds of $Mg_{94}Zn_{2.4}Y_{3.6}$ alloys: the α-Mg grain sizes in the (a) CMC and (b) ICMC alloy; the thicknessess of the network-$Mg_{12}ZnY$ in the (c) CMC and (d) ICMC alloy.

ICMC alloy are also excellent as shown in Fig. 7(c). The yield strength, fracture strength and plastic elongation of the ICMC $Mg_{94}Zn_{2.4}Y_{3.6}$ alloy at 150 °C reach 195 MPa, 302 MPa and 9%, respectively. It is noted that the ICMC alloy didn't show work softening after the yielding at 150 °C.

The fracture morphologies of ICMC specimen tested at room temperature and 150 °C are displayed in Fig. 8. As shown in Fig. 8(a) and (b), there are a large number of cleavage steps which result in the premature rupture on the fracture surface. In addition, a number of dimples, which are the signature of plastic deformation, can be observed on the fracture surface. Therefore, the fracture mode of the ICMC $Mg_{94}Zn_{2.4}Y_{3.6}$ alloy can be classified into the quasi-cleavage fracture. When the samples were tested at 150 °C, the cleavage steps on the fracture surface were obviously decreased and the small dimples
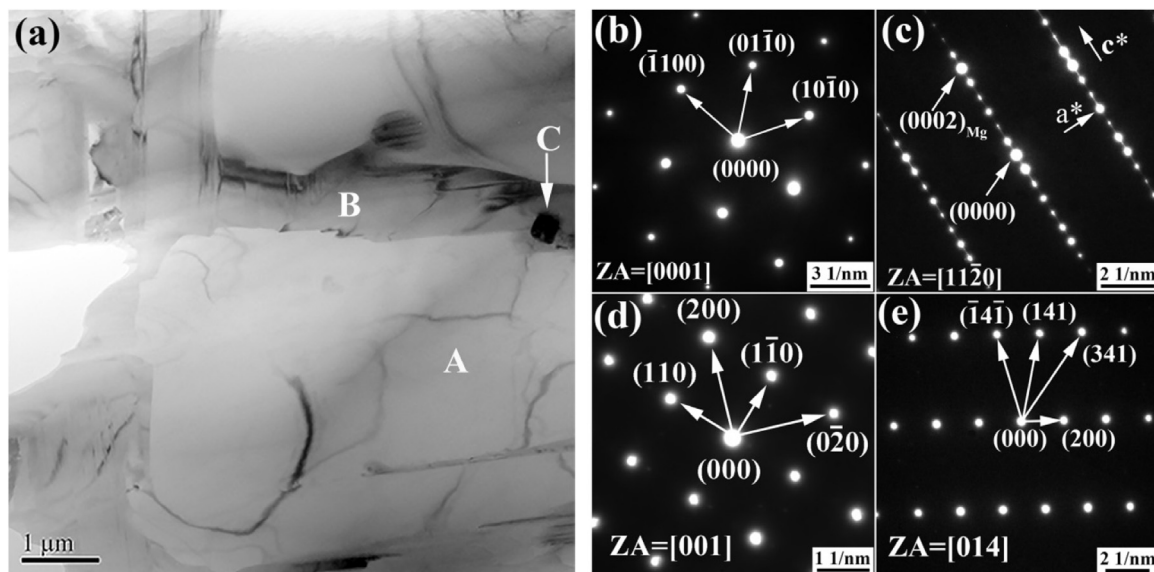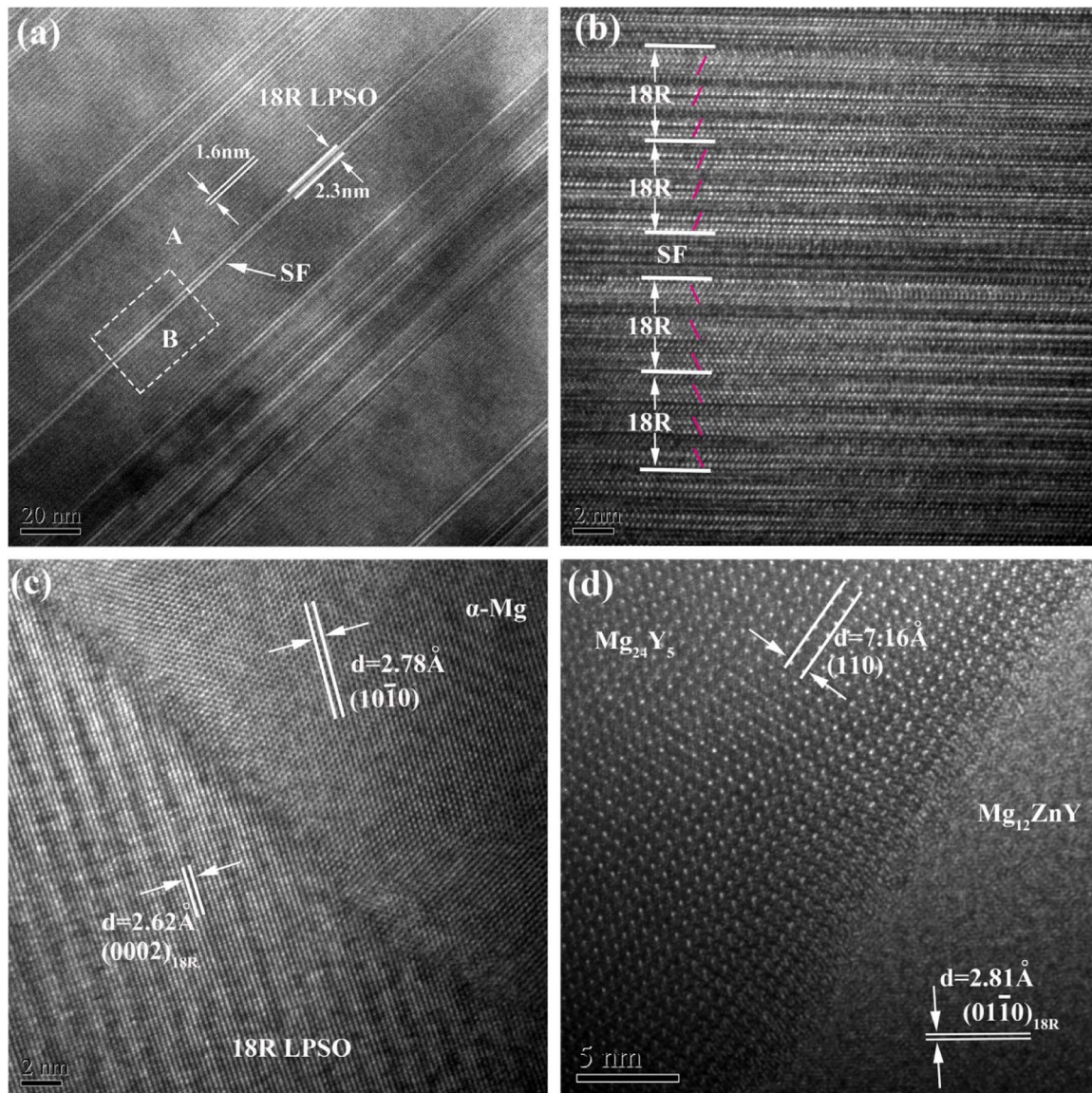

Fig. 5. (a) Bright-field TEM image of the ICMC $Mg_{94}Zn_{2.4}Y_{3.6}$ alloy; (b) the SAED pattern of [0001] zone axis taken from area A; (c) the SAED pattern of the [11$\bar{2}$0] zone axis taken from area B; the SAED patterns taken from area C along the (d) [001] and (e) [014] directions, respectively.

Fig. 6. High resolution TEM (HRTEM) images of ICMC $Mg_{94}Zn_{2.4}Y_{3.6}$ alloy: (a) HRTEM image showing the structure of $Mg_{12}ZnY$ phase; (b) an atomic scale enlargement of the rectangular frame section in (a); (c) HRTEM image of the interface between α-Mg matrix and LPSO phase; (d) HRTEM image of the interface between $Mg_{24}Y_5$ particle and LPSO phase.
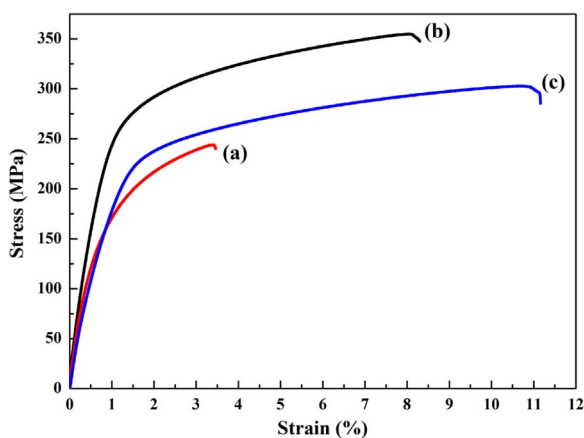

Fig. 7. Engineering tensile stress-strain curves of (a) CMC and (b) ICMC alloy tested at room temperature, (c) ICMC alloy tested at 150 °C.

increased apparently, as shown in Fig. 8(c) and (d). This feature is in accordance with the improvement of the plasticity for ICMC sample. Therefore, the fracture mode for this alloy at high temperature can be considered as ductile fracture. In addition, we also measured the Vickers hardness of these two kinds of alloys, which are HV 87 and HV 112 for CMC and ICMC $Mg_{94}Zn_{2.4}Y_{3.6}$ samples, respectively.

4. Discussion

As shown in Fig. 7, the ICMC $Mg_{94}Zn_{2.4}Y_{3.6}$ alloy exhibits superior tensile mechanical properties compared with CMC alloy. And the enhanced mechanical properties should be attributed to the merits induced by near-rapid solidification process. In the first place, the high cooling rate strongly refines the α-Mg matrix and the $Mg_{12}ZnY$ compound in the ICMC $Mg_{94}Zn_{2.4}Y_{3.6}$ alloy, leading to a significant increase in strength according to the Hall-Petch relationship [8]. Moreover, it is well known that the plasticity could be improved as the grains are refined, which have been proved from Figs. 1 and 7. Secondly, there is obvious solid solution strengthening in α-Mg. As shown in Table 1, the contents of Y and Zn in α-Mg solid solution of ICMC $Mg_{94}Zn_{2.4}Y_{3.6}$ alloy indeed surpass their solubilities. It is known
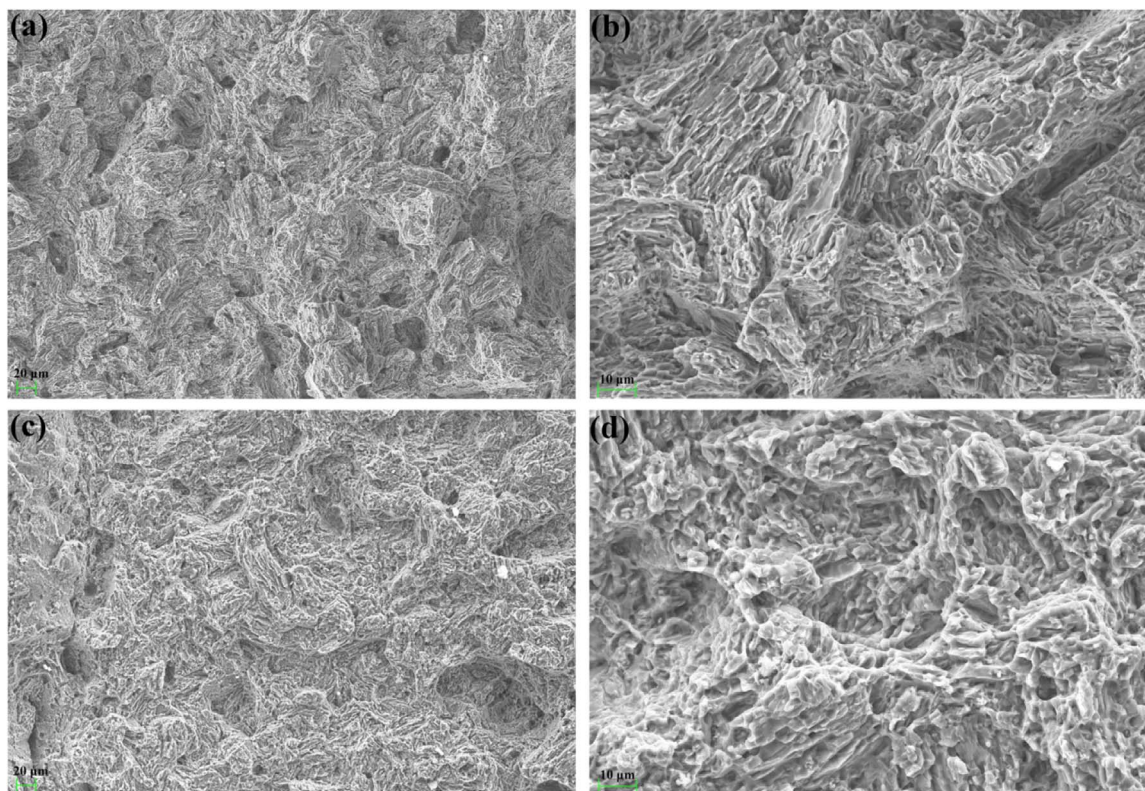
Fig. 8. Typical tensile fracture surface morphologies of the ICMC samples: (a) and (b) tested at room temperature; (c) and (d) tested at 150 °C.

that the atomic radius of Y atom is larger, and the atomic radius of Zn atom is lower than that of Mg atom. This mismatch of the atomic sizes in the α-Mg, induced by dissolved elements, inevitably results in the solid solution strengthening. In addition, the nano-scale $Mg_{24}Y_5$ particles cause a secondary phase precipitation strengthening effect because the interface between $Mg_{12}ZnY$ compound and $Mg_{24}Y_5$ particle is incoherent.

In this work, the refined LPSO phases also exhibit an important strengthening effect. It is not difficult to understand that the deformation mechanism of LPSO phase is similar to that of α-Mg matrix in some aspects. That is, the deformation of LPSO phase may be through the sliding of basal planes along $[11\bar{2}0]$ direction. However, it is more difficult for LPSO to deform since it has long range stacking of basal hexagonal planes with periodic enrichment of Y and Zn atoms in particular atomic planes, which is the distinct difference between the deformability of α-Mg matrixes and that of LPSO phases. Besides, it has been confirmed, as shown in Fig. 6(c), that the interface between LPSO and α-Mg matrix is semi-coherent. It is the above characterizations that make the refined LPSO phases play an important role in the strengthening for the ICMC alloy. As shown in Figs. 1 and 4, the increase of cooling rate for the ICMC alloy not only results in the refinement of α-Mg dendrites, but also decreases the thicknessess of the network-like LPSO phase, *i.e.* the area of interface between LPSO phase and α-Mg matrix is greatly increased. Therefore, it can be deduced that the excellent mechanical properties of ICMC $Mg_{94}Zn_{2.4}Y_{3.6}$ alloy should be attributed to the grain refinement strengthening, the solid solution strengthening, secondary phase precipitation strengthening and crystalline boundaries strengthening.

It is noteworthy that this ICMC alloy still has high strength and work hardening effect at 150 °C, which is beneficial for the application of magnesium alloys at elevated temperature. It has been determined that the melting point of $Mg_{12}ZnY$ phase exceeds 520 °C [32], which ensure its structure stability at high temperature. Moreover, the boundary strength between the α-Mg matrix and the second phase is one of the crucial factors influencing the high temperature strength for

magnesium alloys. Therefore, the semi-coherent interface between LPSO and α-Mg matrix, which has good boundary strength, can have a significant high temperature strengthening effect on the ICMC alloy.

5. Conclusions

(1) The microstructures of both CMC and ICMC $Mg_{94}Zn_{2.4}Y_{3.6}$ alloy are composed of α-Mg dendrites, interdendritic network-$Mg_{12}ZnY$ compounds and a few tiny $Mg_{24}Y_5$ particles. It has been shown that the grain sizes are refined remarkably due to the increase of cooling rate. The α-Mg matrix in ICMC $Mg_{94}Zn_{2.4}Y_{3.6}$ alloy is supersaturated with Y and Zn.

(2) HRTEM study has shown that the microstructure of $Mg_{12}ZnY$ phase is not a simple LPSO, but consists of 18R LPSO and a few of SF. The interface between α-Mg matrix and LPSO phase is semi-coherent with the orientation relationship of $[0002]_\alpha//[11\bar{2}0]_{LPSO}$, $(10\bar{1}0)_\alpha//(0002)_{LPSO}$.

(3) The ICMC $Mg_{94}Zn_{2.4}Y_{3.6}$ alloy exhibits excellent mechanical properties, *i.e.*, high tensile fraction strength of 355 MPa and plastic elongation of 7% at room temperature, and high tensile fracture strength of 302 MPa at 150 °C, respectively.

(4) The strengthening mechanisms of ICMC $Mg_{94}Zn_{2.4}Y_{3.6}$ alloy are mainly attributed to the grain refinements, the solid solution strengthening of α-Mg phase and the secondary phase strengthening of LPSO phases and the crystalline boundaries strengthening induced by the semi-coherent interface between LPSO and α-Mg matrix. Besides, the nano-scale $Mg_{24}Y_5$ particles are also beneficial to the strengthening of this magnesium alloy.

Technology Beijing (2016Z-20).

References

[1] B. Mordike, T. Ebert, Magnesium: properties-applications-potential, Mater. Sci. Eng. A 302 (2001) 37–45.

[2] L.A. Dobrzański, T. Tański, L. Čížek, Z. Brytan, Structure and properties of magnesium cast alloys, J. Mater. Process. Technol. 192–193 (2007) 567–574.

[3] M.K. Kulekci, Magnesium and its alloys applications in automotive industry, Int. J. Adv. Manuf. Technol. 39 (2007) 851–865.

[4] A.A. Luo, Magnesium casting technology for structural applications, J. Magnes. Alloy. 1 (2013) 2–22.

[5] T. Itoi, T. Inazawa, M. Yamasaki, Y. Kawamura, M. Hirohashi, Microstructure and mechanical properties of Mg–Zn–Y alloy sheet prepared by hot-rolling, Mater. Sci. Eng. A 560 (2013) 216–223.

[6] Y. Estrin, A. Vinogradov, Extreme grain refinement by severe plastic deformation: a wealth of challenging science, Acta Mater. 61 (2013) 782–817.

[7] R. Lapovok, X. Gao, J.-F. Nie, Y. Estrin, S.N. Mathaudhu, Enhancement of properties in cast Mg–Y–Zn rod processed by severe plastic deformation, Mater. Sci. Eng. A 615 (2014) 198–207.

[8] N.V. Ravi Kumar, J.J. Blandin, C. Desrayaud, F. Montheillet, M. Suéry, Grain refinement in AZ91 magnesium alloy during thermomechanical processing, Mater. Sci. Eng. A 359 (2003) 150–157.

[9] H. Jones, A perspective on the development of rapid solidification and none-quilibrium processing and its future, Mater. Sci. Eng. A 304–306 (2001) 11–19.

[10] A. Inoue, Y. Kawamura, M. Matsushita, K. Hayashi, J. Koike, Novel hexagonal structure and ultrahigh strength of magnesium solid solution in the Mg–Zn–Y system, J. Mater. Res. 16 (2001) 1894–1900.

[11] Y. Kawamura, K. Hayashi, A. Inoue, T. Masumoto, Rapidly solidi ed powder metallurgy $Mg_{97}Zn_1Y_2$ alloys with excellent tensile yield strength above 600 MPa, Mater. Trans. 42 (2001) 1171–1174.

[12] J. Cai, G.C. Ma, Z. Liu, H.F. Zhang, Z.Q. Hu, Influence of rapid solidification on the microstructure of AZ91HP alloy, J. Alloy. Compd. 422 (2006) 92–96.

[13] E. Mora, G. Garcés, E. Oñorbe, P. Pérez, P. Adeva, High-strength Mg–Zn–Y alloys produced by powder metallurgy, Scr. Mater. 60 (2009) 776–779.

[14] Y.F. Zhao, J.J. Si, J.G. Song, X.D. Hui, High strength Mg–Zn–Ca alloys prepared by atomization and hot pressing process, Mater. Lett. 118 (2014) 55–58.

[15] E. Abe, Y. Kawamura, K. Hayashi, A. Inoue, Long-period ordered structure in a high-strength nanocrystalline Mg-1 at% Zn-2 at% Y alloy studied by atomic-resolution Z-contrast STEM, Acta Mater. 50 (2002) 3845–3857.

[16] M. Matsuda, S. Ii, Y. Kawamura, Y. Ikuhara, M. Nishida, Variation of long-period stacking order structures in rapidly solidified $Mg_{97}Zn_1Y_2$ alloy, Mater. Sci. Eng. A 393 (2005) 269–274.

[17] H. Okuda, T. Horiuchi, T. Tsukamoto, S. Ochiai, M. Yamasaki, Y. Kawamura, Evolution of long-period stacking ordered structures on annealing as-cast $Mg_{85}Y_9Zn_6$ alloy ingot observed by synchrotron radiation small-angle scattering, Scr. Mater. 68 (2013) 575–578.

[18] Z. Luo, S. Zhang, High-resolution electron microscopy on the X–$Mg_{12}ZnY$ phase in a high strength Mg–Zn–Zr–Y magnesium alloy, J. Mater. Sci. Lett. 19 (2000) 813–815.

[19] K. Hagihara, N. Yokotani, Y. Umakoshi, Plastic deformation behavior of $Mg_{12}YZn$ with 18R long-period stacking ordered structure, Intermetallics 18 (2010) 267–276.

[20] X.H. Shao, Z.Q. Yang, X.L. Ma, Strengthening and toughening mechanisms in Mg–Zn–Y alloy with a long period stacking ordered structure, Acta Mater. 58 (2010) 4760–4771.

[21] J. Wang, S. Gao, P. Song, X. Huang, Z. Shi, F. Pan, Effects of phase composition on the mechanical properties and damping capacities of as-extruded Mg–Zn–Y–Zr alloys, J. Alloy. Compd. 509 (2011) 8567–8572.

[22] G. Garces, M.A. Muñoz-Morris, D.G. Morris, J.A. Jimenez, P. Perez, P. Adeva, The role of extrusion texture on strength and its anisotropy in a Mg-base alloy composed of the Long-Period-Structural-Order phase, Intermetallics 55 (2014) 167–176.

[23] Z. Zhang, X. Liu, W. Hu, J. Li, Q. Le, L. Bao, Z. Zhu, J. Cui, Microstructures, mechanical properties and corrosion behaviors of Mg–Y–Zn–Zr alloys with specific Y/Zn mole ratios, J. Alloy. Compd. 624 (2015) 116–125.

[24] H. Fu, X. Geng, High rate directional solidification and its application in single crystal superalloys, Sci. Technol. Adv. Mater. 2 (2001) 197–204.

[25] A. Inoue, A. Kato, T. Zhang, S.G. Kim, T. Masumoto, Mg–Cu–Y amorphous alloys with high mechanical strengths produced by a metallic mold casting method, Mater. Trans. 32 (1991) 609–616.

[26] J. Gröbner, A. Kozlov, X.Y. Fang, J. Geng, J.F. Nie, R. Schmid-Fetzer, Phase equilibria and transformations in ternary Mg-rich Mg–Y–Zn alloys, Acta Mater. 60 (2012) 5948–5962.

[27] A.-P. Tsai, Y. Murakami, A. Niikura, The Zn–Mg–Y phase diagram involving quasicrystals, Philos. Mag. A 80 (2000) 1043–1054.

[28] Y.M. Zhu, A.J. Morton, J.F. Nie, The 18R and 14H long-period stacking ordered structures in Mg–Y–Zn alloys, Acta Mater. 58 (2010) 2936–2947.

[29] Y.M. Zhu, A.J. Morton, J.F. Nie, Growth and transformation mechanisms of 18R and 14H in Mg–Y–Zn alloys, Acta Mater. 60 (2012) 6562–6572.

[30] Y.M. Zhu, M. Weyland, A.J. Morton, K. Oh-ishi, K. Hono, J.F. Nie, The building block of long-period structures in Mg–RE–Zn alloys, Scr. Mater. 60 (2009) 980–983.

[31] M.X. Zhang, P.M. Kelly, Morphology and crystallography of Mg24Y5 precipitate in Mg–Y alloy, Scr. Mater. 48 (2003) 379–384.

[32] Z.H. Huang, S.M. Liang, R.S. Chen, E.H. Han, Solidification pathways and constituent phases of Mg–Zn–Y–Zr alloys, J. Alloy. Compd. 468 (2009) 170–178.